A new method to model magnetic cloud-driven Forbush decreases: the 2016 August 2 event

Simone Benella* [ID],[1] Monica Laurenza [ID],[2] Rami Vainio [ID],[3] Catia Grimani [ID],[1] Giuseppe Consolini [ID],[2] Qiang Hu [ID],[4] and Alexandr Afanasiev [ID][3]

[1]*DiSPeA, Università degli Studi di Urbino Carlo Bo, Via S. Chiara, 27, 61029 Urbino, Italy and INFN, Sezione di Firenze via G. Sansone 1, I-50019, Sesto Fiorentino, Italy*
[2]*INAF-Istituto di Astrofisica e Planetologia Spaziali, Via del Fosso del Cavaliere, 100, I-00133 Roma, Italy*
[3]*Department of Physics and Astronomy, University of Turku, 20014 Turku, Finland*
[4]*Center for Space Plasma and Aeronomic Research, The University of Alabama in Huntsville, Huntsville, AL 35899, USA*

ABSTRACT

Interplanetary coronal mass ejections (ICMEs), generally containing magnetic clouds (MCs), are associated with galactic-cosmic ray (GCR) intensity depressions known as Forbush decreases (FDs). An ICME was observed at L1 between 2016 August 2 at 14:00 UT and August 3 at 03:00 UT. The MC region was identified and its magnetic configuration was retrieved by using the Grad-Shafranov (GS) reconstruction. A weak FD in the GCR count-rate was observed on 2016 August 2 by a particle detector aboard the European Space Agency LISA Pathfinder mission. The spacecraft orbited around L1 and the particle detector allowed to monitor the GCR intensity at energies above 70 MeV n^{-1}. A 9% decrease in the cosmic-ray intensity was observed during the ICME passage. The first structure of the ICME caused a 6.4% sharp decrease, while the MC produced a 2.6% decrease. A suited full-orbit test-particle simulation was performed on the MC configuration obtained through the GS reconstruction. The FD amplitude and time profile obtained through the simulation show an excellent agreement with observations. The test-particle simulation allows to derive the energy dependence of the MC-driven FD, providing an estimate of the decrease amplitude at different rigidities, here compared with several neutron monitor observations. This work points out the importance of the large-scale MC configuration in the interaction between GCRs and ICMEs and suggests that particle drifts have a primary role in modulating the GCR intensity within the MC under study and possibly in at least all slowly expanding ICMEs lacking a shock/sheath region.

Keywords: cosmic rays — methods: numerical — solar-terrestrial relations — Sun: coronal mass ejections (CMEs) — magnetic clouds

1. INTRODUCTION

Forbush decreases (FDs; Forbush 1937) are galactic cosmic-ray (GCR) intensity depressions associated with the passage of interplanetary coronal mass ejections (ICMEs), i.e. large-scale magnetic structures presumably connected to the Sun that during their travel can limit the cosmic-ray propagation. FDs have been traditionally observed through ground-based neutron monitors (NMs) as GCR depressions (e.g., Lockwood 1971; Iucci et al. 1979; Nagashima et al. 1992; Hofer & Flückiger 2000; Signoretti et al. 2011) lasting from several hours to several days, with amplitudes up to about 25%, often exhibiting a two-step decrease profile, which was attributed to the double structure within the associated interplanetary disturbance (Barnden 1973; Flückiger 1985; Iucci et al. 1984, and references therein). As a matter of fact, in the majority of cases at ICME transit it is possible to identify two components: 1) a shock front, followed by a turbulent sheath region, i.e. a sheath of solar wind plasma compressed and shocked, showing large-amplitude fluctuations in magnetic field components (see Cane 2000, and references therein); 2) the magnetic cloud (MC), i.e. a coherent plasma structure characterized by a smooth rotation of the magnetic field components, a

Corresponding author: Simone Benella

*presently at INAF-Istituto di Astrofisica e Planetologia Spaziali, Via del Fosso del Cavaliere, 100, I-00133 Roma, Italy
email: simone.benella@inaf.it

magnetic field strength higher than the background solar wind and values of temperature and plasma-beta that are lower than average (Burlaga et al. 1990; Lepping et al. 1990, 1997). MCs represent a subset of ICMEs presenting a clear signature on the *in situ* spacecraft (S/C) observations.

In general, the most important effect of the ICME passage in generating major FDs is ascribable to the energetic interplanetary shock/sheath region, although it has been proposed that the MC effect could even be dominant (e.g., Sanderson et al. 1990). Intense shocks are associated with the fast ICME propagation and may overcome the MC effect in modulating the GCR intensity, as turbulent magnetic fluctuations within the sheath can influence the GCR propagation significantly (e.g. Wibberenz et al. 1998). However, the minimum intensity occurs after the arrival of the MC (Badruddin 1986; Zhang & Burlaga 1988). For slower ICMEs, the effect of shock and turbulent sheath transit on the GCR intensity could be similar to that associated with the transit and sometimes it could be negligible. Therefore, if no interplanetary shock is found leading an ICME and a weak magnetic field turbulence is observed in the sheath region, the FD evolution mostly depends on the magnetic configuration of the ICME. A statistical study was performed by Richardson & Cane (2011) on more than 300 ICMEs, showing that the 80% of them is associated with a FD, detected by the anti-coincidence guard data on the International Monitoring Platform (IMP-8; Cane 2000), and that the minimum GCR intensities occur within the MC. They also concluded that ICMEs containing MCs cause deeper FDs on average with respect to ICMEs that do not have any MC structure. Despite numerous attempts to relate the properties of FDs with those of ICMEs at 1 au (Richardson et al. 1996; Belov 2008; Belov et al. 2001, 2014; Dumbović et al. 2012) there are significant gaps in our understanding of their underlying physical mechanisms. A renewed interest in studying GCR FDs has been fostered by the most recent S/C observations in the near-Earth space at the lower rigidities with respect to NMs, for which FDs appear larger allowing for the study of the fine structure of the decrease formation. Fore instance, different data sets have been used to study GCRs and the associated FDs recorded by a radiation monitor on board LISA Pathfinder (LPF; Armano et al. 2018), the Electron Proton Helium INstrument detector on board Solar and Heliospheric Observatory (SoHO) and Chandra X-ray observatory (Heber et al. 2015; Dumbović et al. 2018), the anti-coincidence shield of the International Gamma-Ray Astrophysics Laboratory's spectrometer (Jordan et al. 2011). FDs have also been observed at several solar distances by the Radiation Assessment Dosimetry dose rates on the Mars Science Laboratory (von Forstner et al. 2018, 2020; Guo et al. 2018; Papaioannou et al. 2019), the Cassini's Magnetosphere Imaging Instrument and Low Energy Magnetospheric Measurement System measurements (Roussos et al. 2018) and beyond (Witasse et al. 2017; Winslow et al. 2018).

As the effect on the evolution of the GCR intensity does not depend only on the nature of the local magnetic field and solar wind signatures, it is important to consider the large-scale magnetic configuration of the MC, whenever possible, in modulating the cosmic-ray intensity without restricting observations to the magnetic fields that are measured along a particular S/C trajectory during the ICME crossing (Cane & Richardson 2003; Richardson & Cane 2011).

The description of GCR transport in the heliosphere in terms of convection and diffusion is an adequate model to describe large-scale physical phenomena. The same approach can be used on spatial and temporal scales typical of large solar wind disturbances such as ICMEs. One of the general assumptions at the basis of theoretical and numerical studies carried out for FD formation is that closed magnetic structures, simulating the passage of ICMEs and/or MCs, are thought to be empty at the beginning and then are slowly filled due to particle diffusion, thus the Forbush effect is obtained since the strong ICME magnetic fields prevent GCRs from diffusing into them. In this case, physical quantities, e.g. particle distribution and FD amplitude, are computed by solving the particle transport equation in the diffusion approximation (Cane et al. 1995). This approach provides precious clues on this topic, but many evidences reveal that cosmic-ray diffusion only cannot always explain observations (Richardson & Cane 2011). In addition to cross-field diffusion, cosmic-ray adiabatic cooling due to ICME expansion is investigated in Munakata et al. (2006), where the best-fit between the theoretical model and the FD profile measured by a ground-based muon detector network allows to estimate the perpendicular diffusion coefficient. Dumbović et al. (2018) presented an analytical diffusion-expansion model for FDs where the ICME is modeled as an axial magnetic flux-tube expanding from the Sun. In this model cosmic rays penetrate the ICME via perpendicular diffusion and results are in agreement with Cane et al. (1995). Other analytical models based on the diffusion-expansion approach are presented in Arunbabu et al. (2013) and Raghav et al. (2014). In general, results of diffusion-expansion models allow to fit the measured FD amplitude by using the model outcome and thus to estimate the perpendicular diffusion coefficient. In addition to diffusion models, the drift- and full-orbit particle simulations are also widely used in order to investigate properties of high-energy particle propagation. For instance, Krittinatham & Ruffolo (2009) have considered GCR transport through an expanding MC structure computing only drift orbits produced by the typical MC configuration. They

point out that for particle propagation through MC closed field lines the particle drift is strongly effective. This is outlined also by Tortermpun et al. (2018) through the analysis of ground-based GCR observations. On the other hand, the particle diffusion resulting from scattering on magnetic field irregularities appears to play a fundamental role in the particle propagation through a MC structure. In particular, Kubo & Shimazu (2010) showed that, in the case of a non-expanding cylindrical flux-rope model, the ratio between the particle Larmor radius and the MC radius represent a suitable parameter in order to understand whether a cosmic-ray particle can reach the core of the MC or not. Recent works emphasize the importance of MC configurations for the study of the FD formation and time profile (Petukhova et al. 2015, 2017, 2019). In these works the cosmic-ray distribution profile and anisotropies are computed using a toroidal MC model. The particle distribution, calculated from the full-trajectory integration of 10 GeV protons, shows that the MC orientation with respect to the position of ground-based cosmic-ray detectors strongly influence FD observations. Moreover, a technique for the estimate of the MC orientation on the basis of cosmic-ray observations is presented by Kuwabara et al. (2009). The common element present in all of these works is the analytical definition of the MC configuration, supposed to be a symmetrical structure wrapped around a central axis in both cylindrical and toroidal symmetry. These closed structures are well representative of the large-scale MC configuration. An attempt to study an FD due to a realistic MC configuration, taking into account the characteristics of *in situ* IMF and plasma observations, is proposed in the present paper. The large-scale structure of a non-expanding MC is assumed to be axisymmetric and it is retrieved by applying the Grad-Shafranov (GS) reconstruction (Hau & Sonnerup 1999; Hu & Sonnerup 2002; Hu 2017). A numerical approach for reproducing FD evolution due to the passage of MCs is proposed by joining the GS reconstruction with a full-orbit test-particle simulation, representing a powerful method to investigate the effect of the magnetic field structure on cosmic-ray particle propagation. We take advantage of both space- and ground-based observations, as the former allow to detect the fine structure of minor FDs and the latter to investigate the energy dependence of the FD amplitude at the MC transit.

The paper is organized as follows: in section 2 a case-study event is described, data are presented and the GS reconstruction of the MC is provided. The full-orbit test-particle simulation is described in section 3 and model results are compared with observations in section 4. In section 5 discussion and conclusion are provided.

2. THE 2016 AUGUST 2 FORBUSH DECREASE

A faint coronal mass ejection (CME), related to a filament eruption, was observed leaving the Sun off the West limb on 2016 July 28 at 22:24 UT with a linear speed of 265 km s^{-1} as obtained from the SoHO/Large Angle and Spectrometric COronagraph C2 imagery. The interplanetary counterpart was observed at L1 between 2016 August 2 at 14:00 UT and August 3 at 03:00 UT, as reported in the catalog at http://www.srl.caltech.edu/ACE/ASC/DATA/level3/icmetable2.html (see Cane & Richardson 2003, for more details). The ICME structure is apparent in the 1-min data from the Magnetic Field Instrument (MFI; Lepping et al. 1995) and the Solar Wind Experiment (SWE; Ogilvie et al. 1995) on board the NASA Wind S/C, depicted in Figure 1. The magnetic field began to increase at 14:00 UT, reaching 25.2 nT at 01:40 UT on August 3. The solar wind speed fluctuated between 350 km s^{-1} and 465 km s^{-1} during the whole ICME, whereas plasma beta and temperature were low. Within the ICME signatures (as indicated in the Richardson & Cane ICME catalog) only the well-defined MC part was taken into account for the purpose of this study, while disregarding any other substructure. The MC region is clearly distinguishable through the smooth rotation of magnetic field, the low values of plasma-beta and temperature, between 20:10 UTC on August 2 and 03:00 UTC on August 3. Correspondingly, a GCR intensity decrease was observed on 2016 August 2 in space by a radiation monitor on board the LPF S/C, orbiting around the L1 Lagrangian point, and by ground-based NMs.

As the LPF mission aimed to test the instrumentation that will be placed on board the first interferometer for low-frequency gravitational wave detection in space LISA (Laser Interferometer Space Antenna; Amaro-Seoane et al. 2017), a particle detector was placed to monitor the overall galactic and solar cosmic-ray incident flux above 70 MeV n^{-1} charging the free falling test masses for spurious acceleration force noise monitoring (Grimani et al. 2015). The particle detector consists of two ~ 300 μm thick silicon wafers of 1.40×1.05 cm^2 area placed in a telescopic arrangement with a geometrical factor of 18 cm^2 sr for particle single-count measurements. Proton and helium nuclei (constituting roughly 98% of the GCR bulk in the inner heliosphere) were sampled at 0.067 Hz above 70 MeV n^{-1}. Hourly-averaged data allowed for the study of long-term and short-term GCR intensity variations with a statistical uncertainty of 1% (Armano et al. 2018, 2019).

The bottom panel of Figure 1 shows the FD observed in the hourly count rates from LPF between 2016 August 2 and 2016 August 3 associated with the ICME transit. The FD time profile is the result of the modulation from the
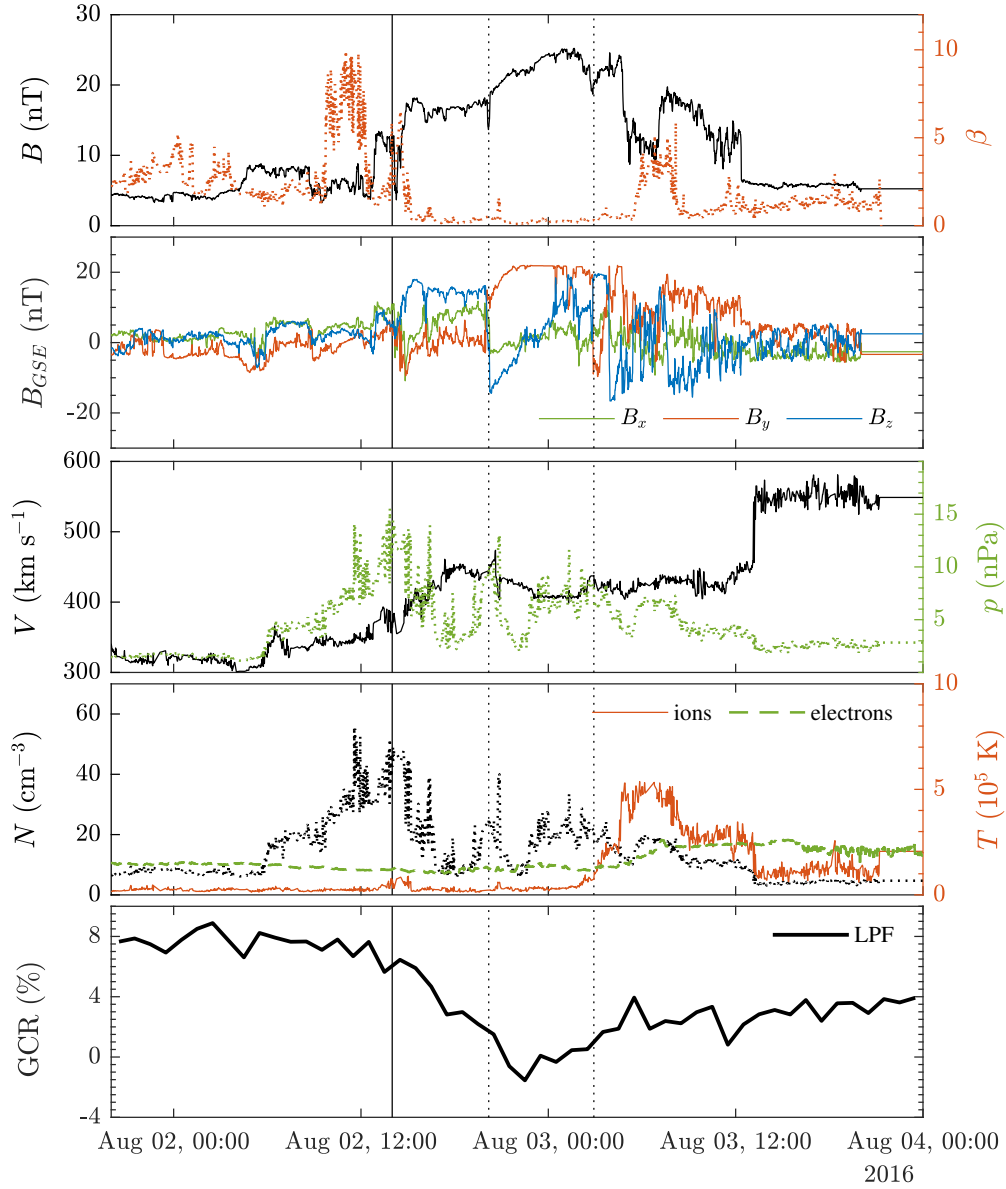
Figure 1. L1 *in situ* data from LPF particle detector (bottom panel) and Wind MFI and SWE observations for the 2016 August 2 event (other panels). The vertical solid line indicates the ICME start time. MC transit time is represented by vertical dotted lines.

two ICME different magnetic regions identified above. The first region is related to the sharp intensity decrease of amplitude $6.4 \pm 1\%$, whereas the MC to the GCR intensity decrease of amplitude $2.6 \pm 1\%$. In Figure 2 are resported the hourly pressure-corrected count rates of several NMs obtained from NM database (www.nmdb.eu). They have been normalised with respect to the average value over the pre-decrease period from 07:00 UTC to 11:00 UTC on 2016 August 2. The FD was observed with few percents amplitudes by the DOMC and South Pole NMs, having a cutoff rigidity of 1.1 GV. On the other hand, no significant decrease was recorded by higher cutoff rigidity NMs, such as Newark (2.36 GV), Rome (6.27 GV), and Mexico City (8.2 GV).

Although the FD commencement appears to be correlated with the passage of the first part of the ICME, we focused on the second step associated with the MC passage. The observation of bi-directional suprathermal electrons by the SWEPAM instrument on board Advanced Composition Explorer (ACE; McComas et al. 1998), as reported in the
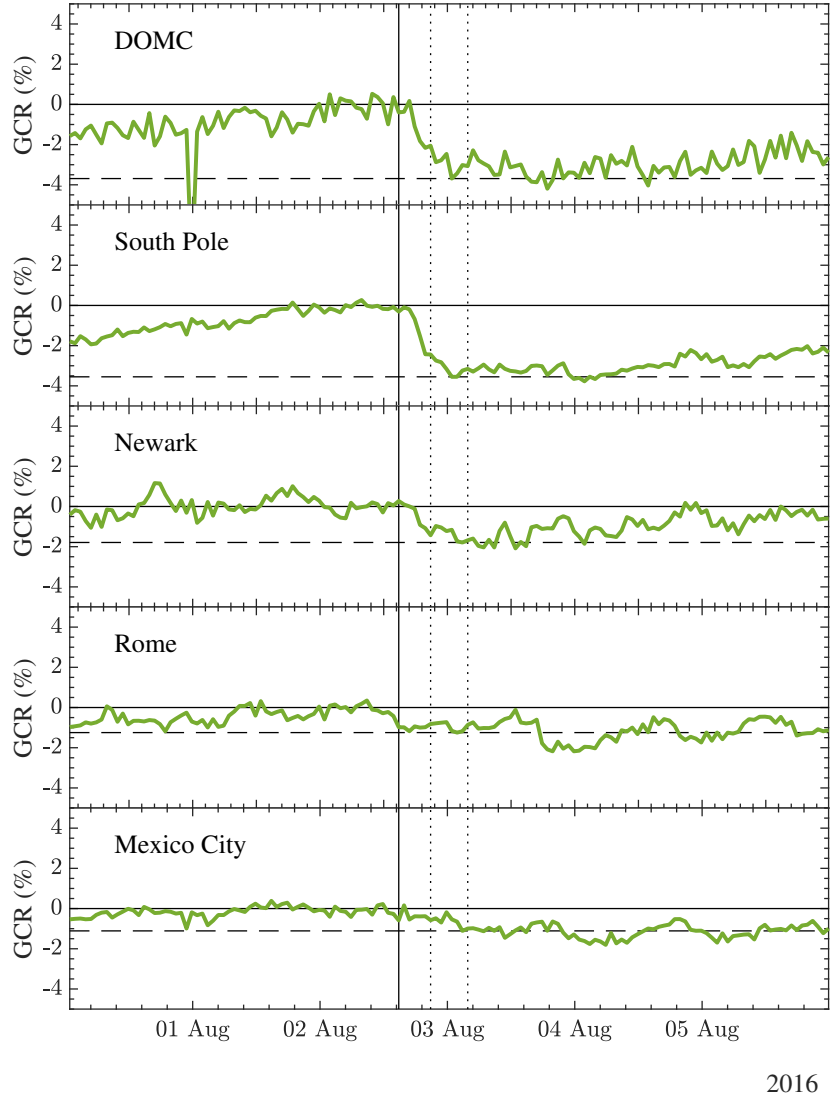
Figure 2. GCR intensity variations gathered by five NM stations for the 2016 August 2 event. The vertical solid line is the arrival time of the ICME at the Earth and the vertical dotted lines are the MC boundaries. The horizontal solid line along zero represents the average pre-decrease count-rate level taken as a reference value to compute FD amplitudes (horizontal dashed lines).

Richardson & Cane ICME catalog, suggests that this MC is a closed plasma structure, for which the GS reconstruction can be applied.

2.1. *Grad-Shafranov reconstruction of the 2016 August 2 flux rope*

The magnetic field structure of the MC was obtained by applying the GS reconstruction by using *in situ* plasma and IMF data from the Wind S/C. This technique is based on the GS equation in Cartesian coordinates:

$$\frac{\partial^2 A}{\partial x^2} + \frac{\partial^2 A}{\partial y^2} = -\mu_0 \frac{d}{dA}\left(p + \frac{B_z^2}{2\mu_0}\right). \tag{1}$$

where A is the vector potential, $\boldsymbol{A} = A(x,y)\hat{\boldsymbol{z}}$, p is the plasma pressure and μ_0 is the vacuum permeability. The equation (1) describes a 2D plasma structure in magnetohydrostatic equilibrium by assuming the axial translational invariance along the z-axis, *i.e.* $\partial/\partial z \approx 0$. Applying the deHoffmann-Teller (HT) analysis (De Hoffmann & Teller 1950; Sonnerup et al. 1987), the optimal HT velocity frame, comoving with the MC at a velocity $\boldsymbol{V}_{HT}$, can be determined. A
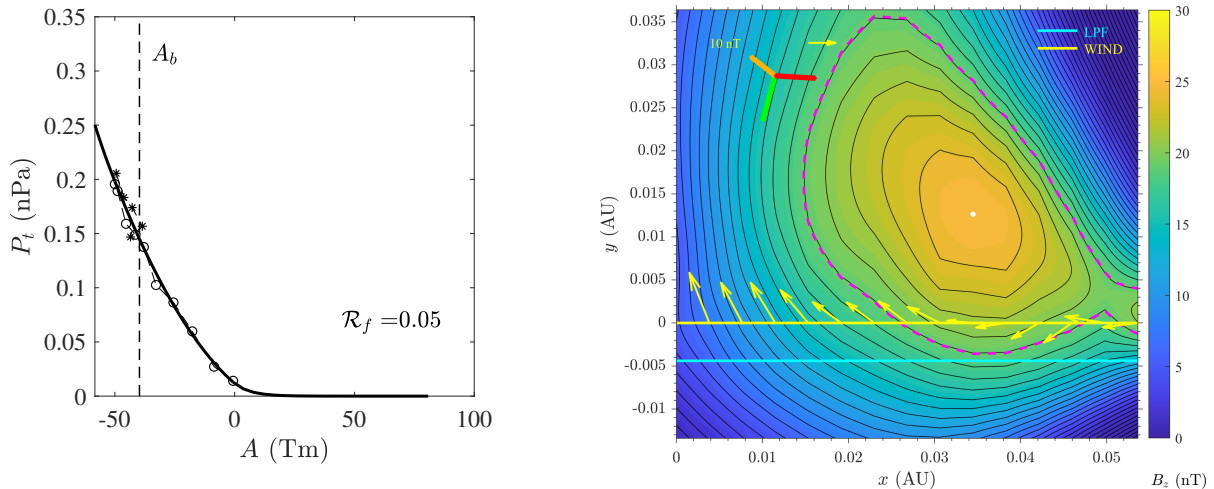
Figure 3. Left: Wind data and fitting curve of $P_t(A)$ for 2016 August 2 MC. Data points represent the S/C measurements for the first half (circles) and for the second half (stars) of the MC crossing. Solid curve represents the fitting function, $P_t(A)$. The fit residue is $\mathcal{R}_f = 0.05$ for this event and $A_b = -44.7$ Tm denotes the boundary value of the vector potential for the double folding of measured data. Right: GS reconstruction of the 2016 August 2 event with Wind (yellow) and LPF (cyan) S/C paths across the MC. The colour plot represents the z component of the magnetic field in the GS reconstruction frame of reference and the solid level curves are the potential vector $A(x, y)$. The dashed magenta line indicates the A_b level curve of the potential and the yellow arrows are the projection of the magnetic field along the Wind S/C path in the x-y plane. A projection of the geocentric solar ecliptic (GSE) reference frame is reported in the corner (x_{GSE} in red, y_{GSE} in yellow and z_{GSE} in green).

good correlation between the convection electric field $-\boldsymbol{V} \times \boldsymbol{B}$ and $-\boldsymbol{V}_{HT} \times \boldsymbol{B}$ indicates that the electric field vanishes and the magnetic structure is stationary, according to the Faraday's law. Thus, the $\boldsymbol{V}_{HT}$ can be considered as the mean velocity of the magnetic structure.

The reconstruction reference frame (x, y, z) is fixed using the condition that the transverse pressure $P_t = p + B_z^2/2\mu_0$ must be as close as possible to a single-valued function of the potential vector A (Hu & Sonnerup 2002). The positive x axis of the reconstruction frame is set according to the direction of the S/C crossing path, located at $y = 0$ by convention, where the magnetic vector potential $A(x, 0)$ is directly evaluated integrating the magnetic field. The transverse pressure $P_t(A)$ is now fitted from the scatter plot of $P_t(x, 0)$ vs $A(x, 0)$ with a combination of analytical functions, exponential and polynomials, to evaluate equation (1) numerically.

Using solar wind plasma and magnetic field measurements from the Wind S/C for the 2016 August 2-3 MC, the HT analysis provides the constant velocity $\boldsymbol{V}_{HT} = (-413.6, -26.4, 11.5)$ km s^{-1}, with a correlation coefficient among the convection electric field and $-\boldsymbol{V}_{HT} \times \boldsymbol{B}$ greater than 0.998. The invariant axis orientation is determined as the minimum residue direction (Hu & Sonnerup 2002). The fit of the transverse pressure as a function of the vector potential is reported in figure 3 (left panel). The GS reconstruction outcome is illustrated in figure 3 (right panel). The orientation of the GSE reference frame with respect to the reconstruction frame in shown in the upper-left corner of the figure. The LPF and Wind paths along the MC are indicated by $y = -4.45 \times 10^{-3}$ AU, cyan solid line and $y = 0$, yellow solid line, respectively. Our results for the reconstructed MC are consistent with those reported in the flux-rope database obtained with Wind S/C data by Hu et al. (2018) and updated on the website http://fluxrope.info/. Note that, as the GS reconstruction does not take into account the dynamics of the MC, it is important to evaluate the deviation between the magnetostatic hypothesis and the observed MC expansion profile. In general, the Grad-Shafranov reconstruction works properly in case of slowly expanding flux-ropes, whereas in case of a clearly expanding flux-rope significant deviations between GS reconstruction predictions and in situ observations can arise and must be discussed (Hu et al. 2005). Here, the assumption that this MC can be treated as a magnetostatic structure in rigid coherent motion with constant HT velocity is tested by computing the expansion velocity $V_{exp} = (V_1 - V_2)/2$, where

$V_1 = 406.6$ km s^{-1} is the velocity at the front boundary of the MC and $V_2 = 421.5$ km s^{-1} the velocity at the back boundary (Möstl et al. 2009). The HT velocity is $V_{HT} = 414.6$ km s^{-1} and the ratio $|V_{exp}|/|V_{HT}| = 0.018 \ll 1$, thus the MC expansion is not particularly significant in the time interval considered for this event.

3. BASICS OF THE FULL-ORBIT TEST-PARTICLE SIMULATION

In order to understand the GCR intensity variation during the MC transit, we performed a full-orbit test-particle simulation by computing the full-particle trajectories on the MC configuration obtained in the previous section. Particles involved in the simulation are only protons, that represent roughly the 90% of the GCR composition in the inner heliosphere. Moreover, an isotropic proton intensity can be reasonably assumed as initial condition for the simulation when a shock/sheath region preceding the MC is lacking. On the other hand, it might not be valid if interplanetary shocks and turbulent sheaths were observed at the leading edge of ICMEs, as they can modify the GCR particle distribution before the passage of the MC due to the diffusion from a highly fluctuating magnetic field (Tortermpun et al. 2018).

The frame of reference of the simulation space is defined according to the reconstruction frame, moving with the MC at a constant HT velocity towards the Earth. Thus, the simulation space is thought as an infinite prism with rectangular section on the x-y plane and side faces parallel to the z-axis. The initial particle positions are randomly selected along the four sides of the GS reconstruction box. Initial velocities are sampled from a given proton energy spectrum (see next section). The directions of the initial velocity vectors are randomly sampled by using the Lambert cosine factor in order to ensure the isotropy of the proton flux entering the simulation space from planar surfaces. Since the z-axis represents the invariant direction of the magnetic structure, boundary conditions along this axis are periodic. The particle propagation is performed by using the relativistic version of the Boris solver (Boris 1970) and particles are tracked until they reach one of the four boundaries of the simulation space. The only contribution to the Lorentz force is due to the magnetic field $\boldsymbol{B}$ because the electric field vanishes according to the HT analysis.

Particles are injected at the GS reconstruction box boundaries that consist of side faces of area A and geometrical factor $A\pi$. An $M \times M$ grid is then defined over the simulation space with cell sizes $(x_{\max} - x_{\min})/M$ and $(y_{\max} - y_{\min})/M$ along the x and y directions, respectively, where the particle fluence is computed after the propagation. If N_E particles with unit weight and energies $E \in [E, E + \Delta E]$ are injected into the simulation space through the surface $A = 2(x_{\max} - x_{\min})L_z + 2(y_{\max} - y_{\min})L_z$, where L_z is the length of the box along the z-axis, the differential fluence at the boundaries is:

$$F^{(in)}(E) = \frac{N_E}{\pi A \, \Delta E}. \tag{2}$$

On the other hand, the isotropic particle differential fluence over the time interval dt in the volume element d^3x as a function of energy is given by:

$$dF(E) = J(E) \, dt = \frac{v}{4\pi} \frac{dN}{d^3x \, dE} \, dt. \tag{3}$$

where $J(E)$ is the proton differential flux. The volume differential fluence computed over the time interval necessary for a particle to pass through the cell C can be written in terms of the discrete quantities used in the test-particle simulation as:

$$F_C(E) = \frac{\sum_{k=1}^{N_{C,E}} n_{C,k} v_k \Delta t}{4\pi \Delta x \Delta y L_z \Delta E} \tag{4}$$

where $\Delta x \Delta y L_z$ is the volume of the cell C and $n_{C,k}$ represents the number of trajectory points associated to the k-th particle crossing the cell C with integration time step Δt and velocity v_k. The number of particles in the cell C with energy in the interval $E \in [E, E + \Delta E]$ is $N_{C,E}$. In order to compute correctly the total number of particle-trajectory points inside each cell, the time step must satisfy the condition $\Delta t_k < \min(\Delta x, \Delta y)/v_k$, that prevents particles from skipping the cell without being counted. In order to set the same time step for all particles we use this condition replacing v_k with the speed of light, i.e. $\Delta t < \min(\Delta x, \Delta y)/c$. Finally, the differential fluence variation in the cell C as, a fraction of the incident fluence, is obtained from equations (2) and (4) as:

$$\Delta F_C(E) = \frac{F_C(E) - F^{(in)}(E)}{F^{(in)}(E)} = \frac{\sum_{k=1}^{N_{C,E}} n_{C,k} v_k (x_{\max} - x_{\min} + y_{\max} - y_{\min}) \Delta t}{2 N_E \Delta x \Delta y} - 1. \tag{5}$$

Since equation (5) provides the normalised hourly-averaged count-rate variations, the proper estimator to be compared with GCR observations is then obtained by integrating the differential fluence variation in energy. Since the test-particle
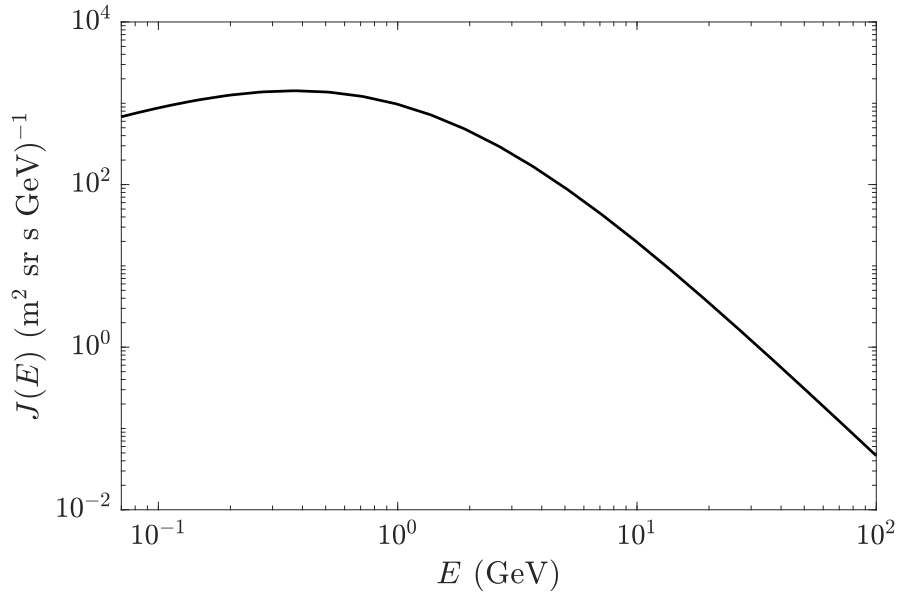
Figure 4. Energy spectrum used in the initialization of the test-particle simulation estimated through the model by Gleeson & Axford (1968)

Table 1. Larmor radii of protons for various particle energies and interplanetary magnetic field observed during the 2016 August 2 FD.

E (GeV)	B (nT)	r_L (AU)	E (GeV)	B (nT)	r_L (AU)
0.1	5	0.002	10	5	0.049
	15	6.59×10^{-4}		15	0.016
	25	3.95×10^{-4}		25	0.010
1	5	0.0075	100	5	0.45
	15	0.0025		15	0.15
	25	0.0015		25	0.09

simulation coordinate system is defined according to the GS reconstruction frame, it is possible to evaluate the fluence variation along the path of a given S/C, represented as a straight line parallel to the x-axis.

4. RESULTS AND DISCUSSION

The method developed in the previous section has been applied in order to reproduce the 2016 August 2 MC-driven part of the FD. Initial particle energies are sampled from the differential proton flux estimated with the Gleeson and Axford model (Gleeson & Axford 1968), where the proton local interstellar spectrum is set according to Usoskin et al. (2017) and the solar modulation parameter is $\phi = 519$ MV, corresponding to August 2016. The computed spectrum is depicted in figure 4 in the energy interval 70 MeV - 100 GeV.

In table 1 are reported the Larmor radii of protons for different values of energy and magnetic field. It appears evident how particles with energy higher than 10 GeV have Larmor radii comparable with the MC size (~ 0.05 AU), thus the guiding center approximation would be inadequate. A selected sample of simulated trajectories for particles of different energies is displayed in Figure 5 (~ 100 MeV top left, ~ 1 GeV top right, ~ 10 GeV bottom left and > 50 GeV bottom right). From the top-left panel of this figure, it can be observed that also 100 MeV energy particles (having small Larmor radii) can reach the core region of the MC and can pass through it, or alternatively be mirrored due to the increasing magnetic field. On the other hand, if a low-energy particle starts to stream along an external
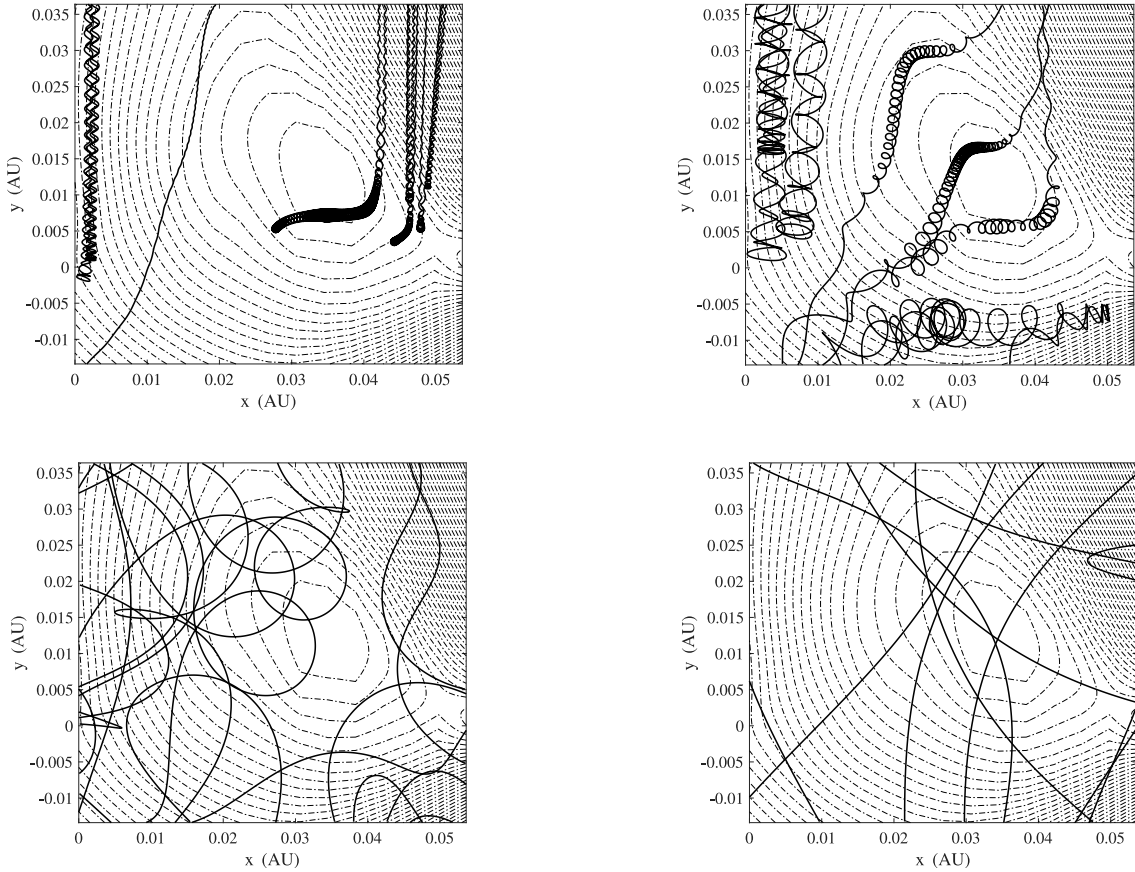
Figure 5. Example of some test-particle trajectories across the MC. Trajectories are projected on the x-y plane for four different energies: ~ 100 MeV (top-left), ~ 1 GeV (top-right), ~ 10 GeV (bottom-left) and ≥ 50 GeV (bottom-right). The dashed lines are the level curves of the vector potential $A(x, y)$.

magnetic field line, it would not be able to reach the inner MC region. In general, whether such low energy particles can reach the MC core depends on the local structure of the magnetic field and the velocity component perpendicular to the field lines. This process is at the origin of the particle drift velocity, possibly causing the GCR intensity decrease observed in the inner region of the MC. On the other hand, higher energetic particles (bottom-left and bottom-right panels in Figure 5) have Larmor radii that are comparable to the size of the structure and can easily pass through the MC core.

Since LPF data are hourly-averaged and the MC transit lasted about 7 hr, the fluence variation is computed on a 7×7 grid on the simulation space with cell size $\Delta x = 0.0077$ AU and $\Delta y = 0.0071$ AU, corresponding to hourly-averaged intensity variations. The proton fluence variation produced by the 2016 August 2 MC is computed by integrating equation (5) in the energy interval 70 MeV - 100 GeV and it is shown in figure 6 (left panel). It can be seen that the minimum values of the proton fluence are obtained around the MC core (with coordinates $x = 0.035$ AU, $y = 0.013$ AU) and on the top-right/bottom-left parts of the map with a decrease amplitude ranging between 2.5% and 4% with respect to the incident fluence. On the other hand, the increase in the proton intensity obtained in the region $x > 0.05$ AU and $y > 0$ can be considered to be a numerical effect induced by the GS reconstruction providing a strong transverse magnetic field in this part of the MC, which holds particles for longer time with respect to other regions.

The simulated fluence variations along the LPF path are displayed in the right panel of figure 6 with respect to GCR measurements on board LPF. For the sake of comparison, the percentage variation is displayed by setting the first data point to zero for both observed and simulated time profiles. An excellent agreement between model and measurements is found. The simulated FD amplitude of 3% is compatible with the measured one of $2.6 \pm 1\%$ within error bars.

The investigation of the FD amplitude energy dependence requires the comparison of our model against the ground-based NM observations (Bachelet et al. 1963; Duldig & Humble 1992; Hofer & Flückiger 2000; Alania & Wawrzynczak
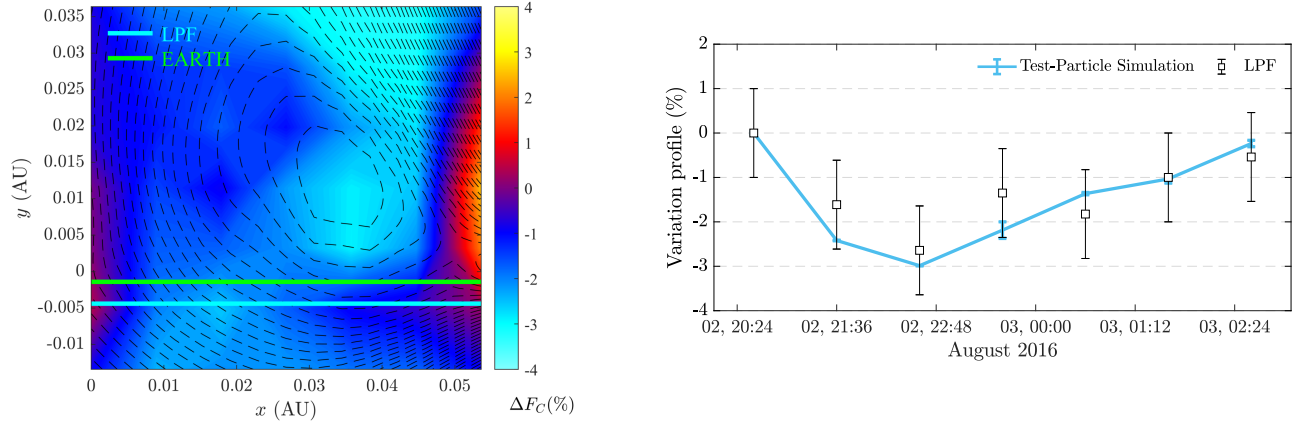
Figure 6. Left: Proton fluence percentage variation obtained from equation (5) in the energy interval 70 MeV - 100 GeV. The black dashed lines are the level curves of the potential vector $A(x, y)$. The cyan (green) solid line is the LPF (Earth) path through the MC. Right: Comparison between the LPF observations and the fluence variation profile obtained from the simulation with standard errors.

2012; Kravtsova & Sdobnov 2013). Hence, the response of a NM to GCRs can be determined by convolution of the GCR primary spectrum with the NM yield function $Y(E)$, which quantifies the response of a standard NM to the unit intensity of primary GCRs with a fixed energy (Clem & Dorman 2000). Thus, the NM count rate $N(E_c)$ computed from the test-particle sample reads:

$$N(E_c) = \int_{E_c}^{\infty} J(E) Y(E) dE \tag{6}$$

where $J(E)$ is the energy spectrum of the simulated particles and E_c is the energy cutoff. To make this calculation we used the yield function proposed by Mishev et al. (2013) at the sea level for protons, derived through the Monte Carlo method. The FD amplitude induced by the MC passage is then computed by using equations (5) and (6) for five energy cutoffs, corresponding to those of DOMC, South Pole, Newark, Rome and Mexico City NM stations, located at different geographic latitudes. The simulated FD amplitudes are listed in Table 2 along with NM characteristics and observations. The effect ascribable to the MC passage identified in GCR intensity (see Figure 2[1]) is a decrease of 1.7% and 1.2% observed by DOMC and South Pole NMs, respectively, whose energy threshold is represented by the atmospheric cutoff of $E_c = 500$ MeV. By setting this threshold energy, the simulation returns a decrease of $1.8 \pm 0.4\%$, which is consistent with observations. Moreover, the MC-driven FD amplitude is weaker for increasing energy of the cosmic-ray particles both in observations and simulations. Amplitudes $< 1\%$ were recorded by higher cutoff energy stations such as Newark, $E_c = 1.6$ GeV, Rome, $E_c = 5.4$ GeV and Mexico City, $E_c = 7.3$ GeV. Similar results are obtained from the simulation that returns FD amplitudes around percent or below at these energies (see Table 2). As a matter of fact, lower energy particles are more affected by the shielding effect originated by the curvature of closed magnetic field lines accompanied by the increasing magnetic field magnitude, whereas particles with energies greater than several GeV can more easily penetrate inside the MC, resulting in a small FD amplitude.

5. CONCLUSIONS

We investigated the effect of the 2016 August 2 MC in modulating the GCR intensity through a new approach which combines GCR observations, the GS reconstruction from *in situ* solar wind and IMF data and a full-orbit test-particle simulation. We used both LPF data in space, which are well suited to study the fine structure of minor FDs, and the ground-based NMs, which allow to investigate the energy dependence of the FD amplitude. The FD amplitude in the LPF hourly count rates at energies > 70 MeV was found to be of 9% with respect to a pre-decrease reference value. In particular, a $6.4 \pm 1\%$ variation was observed in concomitance with the passage of the enhanced magnetic field region within the ICME, whereas an additional $2.6 \pm 1\%$ was observed during the following MC transit. At higher energies

---

[1] In the figure, ICME onset (vertical solid line) and MC transit time (vertical dotted lines) are reported with a proper time-shift, assuming the rigid propagation of the MC structure from L1 to the Earth with constant HT velocity.

Table 2. Geographic latitude, altitude and vertical cutoff rigidities of five NM stations. The total FD amplitudes and the observed variations associated with the MC are reported for the 2016 August 2 event. Simulation results for the MC-driven FD are given with standard error.

	DOMC	South Pole	Newark	Rome	Mexico City
Geographic coordinates	75.06 S, 123.2 E	90.0 S, N/A	39.7 N, 75.8 W	41.9 N, 12.5 E	19.3 N, 260.8 E
Altitude (m)	3233	2820	50	s.l.	2274
Vertical cutoff rigidity (GV)	1.1	1.1	2.4	6.27	8.2
Observed FD amplitude (%)	3.7	2.6	1.8	1.2	1.1
Observed MC-driven FD amplitude (%)	1.7	1.2	< 1	< 1	< 1
Simulated MC-driven FD amplitude(%)	1.8 ± 0.4	1.8 ± 0.4	1.1 ± 0.2	1.0 ± 0.1	0.9 ± 0.1

the NMs recorded lower FD amplitudes of the order of few percents (from 4% at DOMC NM to < 1% at Rome and Mexico City NMs because of the increasing cutoff rigidities), part of which can be attributed to the effect of the MC only for DOMC and South Pole NMs for an amount of 1.7% and 1.2 %, respectively.

We modeled the propagation of the GCR particles in the MC region, as the FD evolution depends on the configuration of the MC. Although the study of the effect of ICME and MC passages on GCR intensity is extensively carried out in the literature with theoretical and numerical models, this work represents the first attempt to join a full-orbit test-particle simulation with the GS reconstruction to study the effect of the GCR intensity modulation due to a large-scale MC, as it provides a realistic large-scale MC structure in terms magnetic field orientation, curvature and gradients over an extended spatial scale.

The 2016 August 2 MC is reconstructed by using Wind MFI and SWE 1-minute resolution data. The dimension of the reconstructed MC is approximately of 0.05 AU and the core of the structure is found to be around the point of coordinates $x = 0.035$ AU and $y = 0.013$ AU with respect to the reconstruction plane, where the axial magnetic field reaches its maximum, $B_z = 25.3$ nT. The z-axis orientation with respect to the GSE is of $\theta = 17.3 \pm 1.7$ and $\phi = 53.9 \pm 2.9$, where θ and ϕ are the latitude and longitude angles respectively.

The simulated particle hourly-averaged intensity variation at the MC passage is calculated along the LPF path and compared with the observations. The amplitude of the simulated FD is found to be 3%, consistent with the $2.6 \pm 1\%$ observed with LPF and the time profile obtained in the simulation shows an excellent agreement with the LPF data trend within error bars. The study of the energy dependence of the GCR intensity response to the MC passage carried out through the simulation reveals that the modulation due to the MC decreases at higher energies as confirmed by NM observations.

The obtained results show that there is a quite efficient transport of particles perpendicularly to the mean magnetic field. As widely known such a cross field transport can be related to the following processes: field line crossings due to drifts and/or scattering and magnetic filed lines random walk due to small-scale magnetic field fluctuations. In the model considered here, particles propagate into the closed MC structure by means of gradient and curvature drifts, whereas magnetic-field fluctuations, possibly leading to cross-field transport as well, are not considered. The good agreement of our simulations with the GCR observations allows us to conclude that small-scale magnetic fluctuations do not play a major role in the cross-field transport of particles inside the MC under study. On the other hand, the characteristics of the GCR intensity modulation associated with the MC passage are governed by the large-scale magnetic field configuration. This study can be considered to be representative of GCR propagation for FDs associated with at least the class of ICMEs lacking a strong shock/sheath region and showing a well-defined and slowly expanding MC, for which magnetostatic equilibrium and isotropy of the GCR intensity entering the MC can be reasonably assumed.

REFERENCES

Alania, M. V., & Wawrzynczak, A. 2012, Advances in space research, 50, 725

Amaro-Seoane, P., Audley, H., Babak, S., et al. 2017, arXiv preprint arXiv:1702.00786

Armano, M., Audley, H., Baird, J., et al. 2018, The Astrophysical Journal, 854, 113

—. 2019, The Astrophysical Journal, 874, 167

Arunbabu, K., Antia, H., Dugad, S., et al. 2013, Astronomy & Astrophysics, 555, A139

Bachelet, F., Balata, P., & Iucci, N. 1963, Il Nuovo Cimento (1955-1965), 27, 425

Badruddin, R. 1986, Solar Phys, 105, 413

Barnden, L. 1973, in International Cosmic Ray Conference, Vol. 2, 1277

Belov, A. 2008, Proceedings of the International Astronomical Union, 4, 439

Belov, A., Eroshenko, E., Oleneva, V., & Yanke, V. 2001, in International Cosmic Ray Conference, Vol. 9, 3552

Belov, A., Abunin, A., Abunina, M., et al. 2014, Solar Physics, 289, 3949

Boris, J. P. 1970, in Proc. 4th Conf. Num. Sim. Plasmas, 3–67

Burlaga, L., Lepping, R., & Jones, J. 1990, Physics of magnetic flux ropes, 58, 373

Cane, H., & Richardson, I. 2003, Journal of Geophysical Research: Space Physics, 108

Cane, H., Richardson, I., & Wibberenz, G. 1995, in International Cosmic Ray Conference, Vol. 4, 377

Cane, H. V. 2000, in Cosmic Rays and Earth (Springer), 55–77

Clem, J. M., & Dorman, L. I. 2000, in Cosmic Rays and Earth (Springer), 335–359

De Hoffmann, F., & Teller, E. 1950, Physical Review, 80, 692

Duldig, M., & Humble, J. 1992, Publications of the Astronomical Society of Australia, 10, 24

Dumbović, M., Heber, B., Vršnak, B., Temmer, M., & Kirin, A. 2018, The Astrophysical Journal, 860, 71

Dumbović, M., Vršnak, B., Čalogović, J., & Župan, R. 2012, Astronomy & Astrophysics, 538, A28

Flückiger, E. 1985, Cosmogenic Nuclides

Forbush, S. E. 1937, Physical Review, 51, 1108

Gleeson, L., & Axford, W. 1968, The Astrophysical Journal, 154, 1011

Grimani, C., Fabi, M., Lobo, A., Mateos, I., & Telloni, D. 2015, Classical and Quantum Gravity, 32, 035001

Guo, J., Lillis, R., Wimmer-Schweingruber, R. F., et al. 2018, Astronomy & Astrophysics, 611, A79

Hau, L.-N., & Sonnerup, B. U. 1999, Journal of Geophysical Research: Space Physics, 104, 6899

Heber, B., Wallmann, C., Galsdorf, D., et al. 2015, Central European astrophysical bulletin, 39, 75

Hofer, M., & Flückiger, E. 2000, Journal of Geophysical Research: Space Physics, 105, 23085

Hu, Q. 2017, Science China Earth Sciences, 60, 1466

Hu, Q., Smith, C. W., Ness, N. F., & Skoug, R. M. 2005, Journal of Geophysical Research-Part A-Space Physics, 110

Hu, Q., & Sonnerup, B. U. 2002, Journal of Geophysical Research: Space Physics, 107, SSH

Hu, Q., Zheng, J., Chen, Y., le Roux, J., & Zhao, L. 2018, The Astrophysical Journal Supplement Series, 239, 12

Iucci, N., Parisi, M., Storini, M., & Villoresi, G. 1979, Il Nuovo Cimento C, 2, 421

—. 1984, Il Nuovo Cimento C, 7, 467

Jordan, A. P., Spence, H. E., Blake, J., & Shaul, D. 2011, Journal of Geophysical Research: Space Physics, 116

Kravtsova, M., & Sdobnov, V. 2013in , IOP Publishing, 012145

Krittinatham, W., & Ruffolo, D. 2009, The Astrophysical Journal, 704, 831

Kubo, Y., & Shimazu, H. 2010, The Astrophysical Journal, 720, 853

Kuwabara, T., Bieber, J., Evenson, P., et al. 2009, Journal of Geophysical Research: Space Physics, 114

Lepping, R., Jones, J., & Burlaga, L. 1990, Journal of Geophysical Research: Space Physics, 95, 11957

Lepping, R., Acūna, M., Burlaga, L., et al. 1995, Space Science Reviews, 71, 207

Lepping, R., Burlaga, L., Szabo, A., et al. 1997, Journal of Geophysical Research: Space Physics, 102, 14049

Lockwood, J. A. 1971, Space Science Reviews, 12, 658

McComas, D., Bame, S., Barker, P., et al. 1998, in The Advanced Composition Explorer Mission (Springer), 563–612

Mishev, A., Usoskin, I., & Kovaltsov, G. 2013, Journal of Geophysical Research: Space Physics, 118, 2783

Möstl, C., Farrugia, C., Miklenic, C., et al. 2009, Journal of Geophysical Research: Space Physics, 114

Munakata, K., Yasue, S., Kato, C., et al. 2006, in Advances in Geosciences: Volume 2: Solar Terrestrial (ST) (World Scientific), 115–124

Nagashima, K., Fujimoto, K., Sakakibara, S., Morishita, I., & Tatsuoka, R. 1992, Planetary and space science, 40, 1109

Ogilvie, K., Chornay, D., Fritzenreiter, R., et al. 1995, Space Science Reviews, 71, 55

Papaioannou, A., Belov, A., Abunina, M., et al. 2019, Solar Physics, 294, 66

Petukhova, A. S., Petukhov, I. S., & Petukhov, S. I. 2015, JETP letters, 102, 697

—. 2017, PoS, 122

—. 2019, Journal of Geophysical Research: Space Physics, 124, 19

Raghav, A., Bhaskar, A., Lotekar, A., Vichare, G., & Yadav, V. 2014, Journal of Cosmology and Astroparticle Physics, 2014, 074

Richardson, I., & Cane, H. 2011, Solar Physics, 270, 609

Richardson, I., Wibberenz, G., & Cane, H. 1996, Journal of Geophysical Research: Space Physics, 101, 13483

Roussos, E., Jackman, C., Thomsen, M., et al. 2018, Icarus, 300, 47

Sanderson, R., Beeck, J., Marsden, G., et al. 1990, in International Cosmic Ray Conference, Vol. 6, 251

Signoretti, F., Laurenza, M., Marcucci, M. F., & Storini, M. 2011, in International Cosmic Ray Conference, Vol. 10, 266

Sonnerup, B. Ö., Papamastorakis, I., Paschmann, G., & Lühr, H. 1987, Journal of Geophysical Research: Space Physics, 92, 12137

Tortermpun, U., Ruffolo, D., & Bieber, J. 2018, The Astrophysical Journal Letters, 852, L26

Usoskin, I. G., Gil, A., Kovaltsov, G. A., Mishev, A. L., & Mikhailov, V. V. 2017, Journal of Geophysical Research: Space Physics, 122, 3875

von Forstner, J. L. F., Guo, J., Wimmer-Schweingruber, R. F., et al. 2018, Journal of Geophysical Research: Space Physics, 123, 39

—. 2020, arXiv preprint arXiv:2003.03157

Wibberenz, G., Le Roux, J., Potgieter, M., & Bieber, J. 1998, Space science reviews, 83, 309

Winslow, R. M., Schwadron, N. A., Lugaz, N., et al. 2018, The Astrophysical Journal, 856, 139

Witasse, O., Sánchez-Cano, B., Mays, M., et al. 2017, Journal of Geophysical Research: Space Physics, 122, 7865

Zhang, G., & Burlaga, L. 1988, Journal of Geophysical Research: Space Physics, 93, 2511